This is a pre-print version associated to paper with doi: **10.1021/acs.jafc.4c05146**

Discovering the ellagitannin landscape of dried walnut shells by liquid chromatography with tandem mass spectrometry

Giovanni Ventura*[1,2], Cosima Damiana Calvano[1,2], Giuliana Bianco[3], Angela Di Capua[3], Ilario Losito[1,2], Tommaso R.I. Cataldi[1,2]

[1] Dipartimento di Chimica, [2] Centro di Ricerca Interdipartimentale SMART, Università degli Studi di Bari Aldo Moro, via Orabona 4, 70126, Bari, Italy, [3]Dipartimento di Scienze, Università degli Studi della Basilicata, Via dell'Ateneo Lucano 10, Potenza, Italy

*Email: giovanni.ventura@uniba.it

This is a pre-print version associated to paper with doi: **10.1021/acs.jafc.4c05146**

Abstract

Walnut shells, often discarded as waste, hold hidden potential as a source of ellagitannins (ETs), compounds known for their promising antioxidant properties and health benefits. This study employed reversed-phase liquid chromatography (RPLC) coupled with Orbitrap-based high-resolution mass spectrometry (HRMS) via electrospray ionization (ESI) in negative polarity to investigate the ET profile in extracts of dried powdered walnut shells. Several compounds belonging to various ET families were successfully identified as deprotonated molecules ($[M-H]^-$) and characterized, including mono-, di-, tri-, tetra-, and pentagalloyl glucopyranoses, as well as ETs containing the hexahydroxydiphenoyl (HHDP) group. Characteristic product ions were identified in HR tandem MS spectra and employed to recognize the ET landscape. Analysis revealed a complex picture~~,~~ with more than 10 isomers identified in some cases. However, the structural similarity and limitations in MS/MS data hindered the definitive identification of all isomers. Characterization of ETs featuring HHDP groups also remained challenging. Despite these restraints, the estimated total content of ETs suggests potential application in the food, pharmaceutical, and cosmetic industries of those extracts. These findings indicate that walnut shells can be considered a sustainable source of health-promoting compounds, contributing to a greener economy.

Keywords: Ellagitannins, walnut shells, RPLC-ESI-MS, tandem MS, wastes.

This is a pre-print version associated to paper with doi: **10.1021/acs.jafc.4c05146**

1. INTRODUCTION

Wastes from fruits and vegetables contain valuable bioactive compounds that can be used in various industries as food additives, pharmaceutical excipients, textile dyes, and biofuel production [1–4]. Most of these compounds are secondary metabolites that act as antioxidants, aid in energy production or are involved in protein synthesis [5,6]. Often, these compounds are concentrated in the outermost, non-edible parts of fruits and vegetables, which become waste during processing [6]. Their structural complexity may explain why most researchers have focused on a few abundant classes of compounds, while studies on their preventive action against lifestyle-related diseases are still limited.

The word "walnut" refers to the edible seed of any tree in the *Juglans* genus, with the most common being the English walnut (*Juglans regia*). Interestingly, humans have been appreciating walnuts for centuries, not just for their taste, but also for their potential health benefits [7–9]. The edible part of the walnut is rich in nutrients such as polyunsaturated fatty acids, proteins, minerals, flavonoids, polyphenols and phenolic acids [8]. Walnut shells hold a special class of antioxidant compounds called ellagitannins (ETs) [10,11]. Even more fascinating, the amount of ETs can vary depending on the type of walnut trees and the environment they grow [12].

ETs are a class of natural polyphenols derived from the secondary metabolism found in many flowering plants (*Angiosperms*), particularly those with two seed leaves (dicotyledons) [13]. They are composed of a central glucopyranoside core with units of gallic acid (GA) linked by ester bonds (see **Figure 1**). Sometimes, these GA units can also link directly to each other by biaryl C-C and C-O bonds resulting from inter- and intra-molecular phenolic oxidative coupling processes [14–16]. After ingestion, ETs release ellagic acid ($C_{14}H_6O_8$), which is converted by the intestinal microflora to urolithin A and other derived metabolites [17–20].

ETs offer a variety of health benefits; they act as antioxidants, fighting harmful free radicals that help to prevent diseases like cancer, heart diseases, and neurodegenerative disorders [17,21]. More than 500 different ETs from various plant sources have been reported using several analytical techniques [22–25]. ETs encompass a broad range of structures, including monomeric ETs, C-glycosidic ETs with an open-chain glucose core, complex tannins formed by the condensation of C-glycosidic tannins with flavan-3-ol, and oligomers produced through intermolecular C-O or C-C bonds between monomeric units[26]. Therefore, studying ETs, in various foods and bodily fluids, can be tricky. In the early stages of ET research, colorimetric analyses were widely utilized [27]. Additionally, the acid hydrolysis releases ellagic acid, which is easier to measure, but this metabolite can react with other compounds, complicating the picture [17]. Subsequently, various methods based on liquid chromatography (LC) have been extensively employed for the analysis of ETs, often utilizing UV-Vis analysis and/or mass spectrometry [27–30]. Also, the use of ^{1}H and ^{13}C NMR analyses has been reported, although it necessitates a prior separation and purification step of possible isomers [31].

In a prior study, examining the phenolic fraction and fatty acids extracted from walnut shells, we noted a significant increase in the content of ETs, especially bis HHDP-Glucose (bis-hexahydroxydiphenoyl (HHDP) glucopyranose), following fine grinding with ball milling [32]. This study explores the potential of walnut shell wastes as a source of valuable ETs. Reversed-phase LC (RPLC) coupled with MS by electrospray ionization (ESI) in negative polarity was successfully applied to investigate the complexity and diversity of these secondary metabolites in extracts of dried powdered walnut shells.

2. MATERIALS AND METHODS

2.1 Chemicals. Water (H_2O), acetonitrile (ACN), methanol (MeOH), formic acid (LC-MS grade), ammonium formate (reagent grade), ellagic acid (≥95%, HPLC), and 1,3,6-tri-O-galloyl-beta-D-glucose (≥95%, LC/MS-ELSD) were purchased from Merck (Milan, Italy). Absolute ethanol (EtOH) was obtained from Panreac (99.8% v/v). Standard solutions for negative and positive calibrations of MS instrumentations were obtained from Thermo Scientific (Waltham, MA, USA).

2.2 Nomenclature of ellagitannins. In this study, hydrolysable tannins are named using the following convention: GP represents glucopyranoside, GA is gallic acid, and HHDP is the hexahydroxydiphenoyl group. The numbers indicate either the position of the substituent on glucopyranoside (if preceding GA or HHDP) or the number of gallic acid units attached to glucopyranoside (if following GA or HHDP). Thus, GA_2HHDP_2-GP represent digalloyl-dihexahydroxydiphenoyl glucose, while ^{6}GA-GP is 6-O-galloyl-glucose.

2.3 Sample Preparation. Walnuts from Apulia (Italy), provided by a local farmer, were processed to obtain walnut shell powder following the procedure previously reported [33]. Initially, dried walnut shells underwent coarse fragmentation and were subsequently sieved through a 1 mm sieve. The resulting fragments underwent further size reduction using a planetary ball miller (Fritsch Pulverisette 7 planetary micro mill)[32]. Throughout the milling process, the temperature was maintained below 50 °C. Subsequently, the resulting biomass was sieved using a 0.5 mm sieve. Samples were subjected to Soxhlet extraction [34] for 12 hours using ethanol, with the extraction temperature reaching 78 °C. Approximately 300 mg of the product were dissolved in 20 mL of water/MeOH 1:1 and centrifuged. The supernatant was

then diluted 1:10 in the initial mobile phase composition and directly injected into the instrument. A standard solution of ellagic acid was prepared at a concentration of 0.5 mg/mL in ethanol. This solution was then diluted 1:10 with the initial mobile phase composition for chromatographic analysis.

2.4 Instrumentation and operating conditions. Samples were analyzed by using an Ultimate 3000 UHPLC system (Thermo Scientific, Waltham, MA, USA) coupled to a Q-Exactive Orbitrap™ analyzer or a Velos Pro mass spectrometer including a Linear Ion Trap analyzer (LIT), both from Thermo Scientific, Waltham, MA, USA. The column effluent was transferred into the spectrometers through a heated electrospray ionization (HESI) interface. The main electrospray and ion optics parameters were the following: sheath gas flow rate, 35 arbitrary units (a.u.); auxiliary gas flow rate, 15 a.u.; spray voltage, -3.5 kV (negative polarity); capillary temperature, 320°C. S-Lens RF Level was set at 60 a.u. for Velos Pro analyses and 100 a.u. for Orbitrap ones. HCD-MS/MS and CID-MS^3 analyses were performed using the Q-Exactive and the Velos Pro spectrometer, respectively, using a 1 *m/z* unit-wide isolation window centred on the *m/z* ratio of the precursor ion and setting a Normalized Collisional Energy (NCE) value of 30%, in the former case, and of 35 % in the latter one. The resolution settings used during the analyses are as follows: 70,000 at m/z 200 for full HR-MS and 17,500 at m/z 200 for HR-MS/MS analyses.

LC separations were performed using a conventional ODS Ascentis® Express column (150 x 2.1 mm ID, 2.7 µm particle size), equipped with a pre-column (10 x 2.1 mm ID) (Merck, Milan, Italy). The column temperature was maintained at 30°C and a constant flow rate of 0.25 mL/min was employed. 5.0 µL of walnut extract were injected using an autosampler. The following binary elution program, based on water (solvent A) and ACN (solvent B), both

containing 0.1% (v/v) of formic acid, was adopted: 0-1 min: isocratic at 2% solvent B; 1-5 min: linear gradient from 2 to 8% v/v solvent B; 5-20 min: linear gradient from 8 to 17% v/v solvent B; 20-25 min: linear gradient from 17 to 85% v/v solvent B; 25-30 min: isocratic at 85% solvent B; 30-35 min: return to initial composition, followed by 5 min of equilibration.

2.5 Quantitative analyses. Calibration curves using 1,3,6-tri-O-galloyl-beta-D-glucose were explored in the range 1.0–20.0 µM by preparing standard mix solutions at six concentration levels (1.0, 2.5, 5.0, 10.0, 15.0 and 20.0 µM each). Three injection replicates were analyzed. Limits of detection (LOD) and quantification (LOQ) were respectively calculated as three- and ten-fold of the ratio between the standard deviation of the intercept and the slope of the calibration curves obtained in pure solvents.

2.6 ETs annotation. For this study, a manual approach was used to identify compounds within the chromatogram. An internal database of potential *m/z* values for the investigated species was compiled, and these values were searched in the HR-MS spectra with an accuracy of ≤ 5 ppm to construct the extract ion current (EIC) chromatograms. The MS/MS spectra for each detected peak were then manually analyzed, focusing on finding diagnostic product ions with a maximum allowable error of 5 ppm. The occurrence of *m/z* 300.999 $[C_{14}H_5O_8]^-$ was searched for HHDP-, HHDP, and GA-containing species, while *m/z* 169.014 $[C_7H_5O_5]^-$ was investigated for GA-containing species. Spectra containing product ions documented in the literature and easily assignable to isobaric species were ruled out. In the MS/MS spectra, all fragments listed in the table with intensities above the 5% threshold were manually annotated with tentative identifications that are consistent with the proposed structures and compatible with the precursor's formula.

According to the criteria indicated by Schymanski et al. [35], the identifications were provided as tentative candidates (i.e. Level 3), except for 1,3,6-tri-O-galloyl-beta-D-glucose and ellagic acid, whose structures were confirmed by standards injections (Level 1).

3. RESULTS AND DISCUSSION

3.1. RPLC separation and HRMS and MS/MS characterization of HHDP containing ETs.

ETs feature a GP core which forms ester bonds with varying numbers of GA molecules or with GA derivatives (see **Figure 1**). For example, many ETs include the hexahydroxydiphenoyl (HHDP) group [15], which is formed by the intramolecular oxidative C–C coupling of spatially close galloyl residues, such as those in position 4,6, 2,3, or 3,6 on the GP core [15]. The HHDP residue can bind to the GP core at both adjacent and non-adjacent positions, as reported in **Figure S1**, and, upon acidic hydrolysis, ellagic acid is released as reported by Guo *et al*. [36]. Recently, we described the occurrence of a bis-HHDP-glucopyranoside ($HHDP_2$-GP) among the predominant hydrolysable tannins of dried walnut shells[32]. Among the theoretically conceivable isomers of $HHDP_2$-GP, pedunculagin (position binding in 2, 3 and 4, 6; see structure 3 in **Figure S1**) has caught significant attention in the literature due to its potential anti-tumour and anti-atherosclerotic activities [37,38]. Given the numerous structural isomers and the lack of commercially available standards, a chromatographic method is demanded to investigate ETs' complexity.

Figure 2A shows the EIC chromatogram (EICC) of a sample extract from dried, powdered walnut shells. The EICC was obtained by electrospray ionization (ESI) in negative polarity at *m/z* 783.069, corresponding to the deprotonated species $[HHDP_2\text{-GP-H}]^-$ (orange). In the chromatograms, isomers are indicated by the same letter but different numbers, with the numbers reflecting their retention times in ascending order. Although ETs can also ionize

in positive ion mode as $[M+H]^+$, $[M-H_2O+H]^+$, $[M+Na]^+$, $[M+NH_4]^+$ species (see **Figure S2A**), the ionization efficiencies were relatively lower than negative polarity, as apparent from the comparison of intensity scales in **Figures A and S2B** using the same sample. Indeed, even summing the ion currents for signals at *m/z* 767.073, *m/z* 785.083, *m/z* 802.110, and *m/z* 807.065, obtained in positive ion mode, the EICC peak intensity was approximately half compared to the deprotonated species at *m/z* 783.069. Thus, the subsequent analyses were carried out in negative polarity.

Tandem MS spectra were collected to identify useful product ions and distinguish between isomeric species, as shown in **Figure 3** for the most abundant isomers of HHDP_2-GP, corresponding to peaks labelled #3a and #4a. Tandem MS spectra of #3a and #4a exhibited the same main signals, with accurate *m/z* values at 481.062, 300.999, 275.020, and 249.041. While the peak at *m/z* 481.062 is due to the gas-phase formation of HHDP-glucopyranoside ($[HHDP\text{-}GP - H]^-$), the most intense peak of both spectra was found at *m/z* 300.999 ($[C_{14}H_5O_8]^-$, see inset of **Figure 3A**). The suggested structure of product ion at *m/z* 275.020 ($[C_{13}H_7O_7]^-$) is reported in the inset of **Figure 3B**. All these product ions are diagnostic of *pedunculagin isomers* [18,39], but information on the linking position of the HHDP moiety on the GP core is not provided. Tandem MS spectra of species #1a and #2a (**Figure S3**) were richer in signals, with the peak at *m/z* 299.020, consistent with the chemical formula $[C_{15}H_7O_7]^-$ being the base peak in both spectra. A similar set of signals was observed in the two spectra, the only exception being the one at *m/z* 481.062. These outcomes suggest the occurrence of isobaric species identified as a quercetin derivative [40], not further investigated in this work.

Another important ET found in the ethanolic extract of dried walnut shells, detected at *m/z* 481.062, was identified as HHDP-GP. Excluding anomers, which would double the number of isomers, there are seven potential structural isomers for this species: four with HHDP bound

to adjacent core positions, and three exhibiting a 1,3 interaction. While some of the observed peaks could be due to anomeric species, the complexities of studying these diastereoisomers, particularly since their proportion can vary with the solvent[41], have deterred us from attempting to identify the precise anomeric forms present in the sample. In a study by Grace et al.[42], a specific extraction process led to compounds with an unsubstituted anomeric proton appearing as double peaks under certain chromatographic conditions, indicating epimeric mixtures. In contrast, ETs with substituents at the 1-position appeared as single peaks. This suggests that the extraction method influences anomer prevalence, especially for ETs with an unsubstituted C1, or that chromatographic separation might cause peak splitting and favour one anomer over another. Although this aspect is important, it was not explored further in the current study.

The blue profile shown in **Figure 2A** exhibits three poorly resolved chromatographic peaks at low retention times, due to the relatively high polarity of these secondary metabolites. In all tandem mass spectra of the precursor ion at *m/z* 481.062 the most intense signal corresponded to the ion at *m/z* 301.000 alongside the one at *m/z* 275.021 (see **Figure S4**). Additionally, an interesting, yet low-intensity, peak signal was observed at *m/z* 421.043 only for chromatographic peak #2b. The neutral loss of 60.021 Da suggests that the hydroxyl group at position 6 of the glucopyranose core is likely free, causing a neutral loss of $C_2H_4O_2$ which most likely involves C^5 and C^6 (*vide infra*).

As the number of GA and HHDP moieties increases, the structural complexity increases as well. Indeed, ETs characterized by the simultaneous presence of the HHDP group and GA can be found. An example is HHDP-GA-GP, which may be useful for treating inflammatory complaints[43], whose EICC at *m/z* 633.073 is reported in **Figure 2A** (green). Ten chromatographic peaks were observed in this case, with peaks #6c and #9c being the most

abundant. Excluding anomers, it is not surprising that there are at least 24 potential isomers. This count does not include tannins where the gallic acid (GA) moiety is not bridged by the carboxylic group or the hexahydroxydiphenoyl (HHDP) group. In all the MS/MS spectra obtained for *m/z* 633.073, whose information is reported as a heatmap in **Figure 4**, the base peak was found at *m/z* 300.999, i.e. the diagnostic ion of the HHDP group reported in **Figure 2**. This peak predominates over the GA loss, observed both as ketene ($[M\text{-}GAk\text{-}H]^-$ at *m/z* 481.062) and as an intact molecule ($[M\text{-}GA\text{-}H]^-$ at *m/z* 463.053). Except for isomers #9c and #10c, the intensity of the $[M\text{-}GAk\text{-}H]^-$ ion is consistently higher than intact GA loss, suggesting that adjacent positions to the galloyl group are free. The peak signal at *m/z* 249.041 of species #1c and #2c is significant and suggests the double decarboxylation of the HHDP group, as reported by Bowers et al. [44]. Moreover, the signal at *m/z* 421.031 $[M\text{-}212]^-$ is particularly intense for species #5c and #7c.

In all tandem MS spectra referred to deprotonated HHDP-GA_2-GP, whose EICC at *m/z* 785.084 is displayed as a blue profile in **Figure 2B**, with four peaks labelled (#1e-#4e), the ion at *m/z* 300.999 represented the base peak (**Figure 4**), revealing that those species are Tellimagrandin I and its isomers. Tellimagrandin I is an intriguing compound found in almond skin, holding liver-protective properties, specifically by suppressing damage caused by carbon tetrachloride in hepatocytes [45]. The isomer labelled #5c exhibited the gas phase neutral loss of GA as ketene (GAk), yielding deprotonated HHDP-galloyl-glucopyranoside ($[HHDP\text{-}GA\text{-}GP\text{-}H]^-$) at *m/z* 633.073 (see **Figure 4**). The neutral loss of HHDP as ketene, leading to the formation of the ion at *m/z* 483.078, is drastically less important in this spectrum. No further clues regarding the relative positions of GA and HHDP substituents on the GP core can be inferred, but it can be assumed that in this case the galloyl group is located at a more reactive position, prone to be released under tandem MS. It is also possible that these are isomers

where the gallic acid molecules are bound differently to positions postulated so far.

As expected, the $HHDP_2$-GA-GP and HHDP-GA_3-GP species, detected respectively at *m/z* 935.080 and 937.095 (see the orange and green EICCs in **Figure 2B**, respectively) exhibited relatively greater retention times. In these cases, doubly charged ions, detected at *m/z* 467.036 and 468.044, respectively, were predominantly obtained, and thus used to obtain a multi-EICC profile for each of both species. The MS/MS spectra of both precursor ions #1d and #2d are shown in plots A and B of **Figure 5**, respectively. Among the HHDDP-GA_3-GP isomers, Tellimagrandin II, also known as Eugeniin, was found in almond skin and shares the same properties as Tellimagrandin I [45]. Kurokawa et al. [46] reported Eugeniin as a compound exhibiting anti-herpes virus properties. While the tandem mass spectrum of #2d (plot **5B**) showed two main product ions at *m/z* 301.000 and *m/z* 275.021, further less intense but interesting peaks were observed for #1d, as evidenced in **Figure 5A**. Among them, the one at *m/z* 633.073 was ascribed to the loss of HHDP as ketene. A peak signal at *m/z* 299.021 was also detected, by analogy with tandem MS spectra referred to species #1a and #2a (see **Figure S3**). Based on the considerations made for the latter, the presence of isobaric and/or isomeric species is suggested also for the precursor ion at *m/z* 935.080 and it was not further investigated. One of the most substituted ETs found in extracts of dried walnut shells was observed at *m/z* 937.095, containing both HHDP and GA groups. The tandem MS/MS spectra referred to species #1f and #2f, sharing this *m/z* ratio, are reported in **Figure S5**. Both spectra were very similar, exhibiting some of the peak signals already discussed for other ETs. The most intense signals were at *m/z* 300.999 and *m/z* 275.020, followed by *m/z* 249.041 and *m/z* 169.015. A peak at *m/z* 785.084, corresponding to the loss of GAk, was also annotated.

Since ellagic acid can be generated from tannin species, its occurrence was investigated in the ethanol extracts of dried walnut shells. Ellagic acid is a natural phenolic

compound, found abundantly in various plant species and fruits like strawberries, raspberries, and grapes, which exhibits antimutagenic and antioxidant properties [47,48]. The EIC chromatogram at *m/z* 301.000 revealed a significant peak of deprotonated ellagic acid at around 22.5 minutes (see **Figure S6A**). Further confirmation of this compound's identity was achieved through standard injection (see **Figure S6B**) and tandem MS (data not shown). The presence of ellagic acid in wasted walnut shells is a significant finding that improves the value of this byproduct.

3.2. Characterization of ETs containing GA

Monogalloylglucopyranoside (GA_1-GP) is the forerunner of ETs. As its name implies, it comprises a GP core with a GA substituent condensed with one of the five accessible hydroxyl groups. Again, excluding anomers, five putative structural isomers can be considered for this compound (see **Figure S7**), each with a substituent esterified to one of the hydroxyl groups. Considering the closed form of the GP core with five hydroxyl groups at positions (1, 2, 3, 4, 6) and only one anomeric form, the number of possible isomers (*n*) when different galloyl moieties are linked to the GP core is calculated by the formula $n = 5!/(GA!\times(5\text{-}GA)!)$, where *GA* represents the number of galloyl substituents. In the fifth column of **Table 1** are listed the numbers of possible combinations of species resulting from multiple GA moieties linked to GP core with the chemical formula and the monoisotopic masses of deprotonated species. Once more, anomers were excluded from the calculation.

Figure 6A displays the EIC chromatogram by RPLC-ESI(-)-FTMS of deprotonated ETs corresponding to two types of GA_n-GP species, namely GA_1-GP (orange) and GA_2-GP (blue), at *m/z* 331.067 and 483.078, respectively. It is important to emphasize that the signal intensity is ten times lower than that of **Figure 2**, thus reflecting the lower content of these ETs in the

sample extracts of dried walnut shells. The analysis successfully identified five distinct chromatographic peaks for GA_1-GP (#1g-#5g). Interestingly, four of these peaks appeared within the first 4 min, while the fifth one eluted at 7.3 min. This difference in retention time can be explained by the possibility that the later-eluting isomer has the GA unit attached at the 6' position of the GP core (structure ***E*** in **Figure S7**). This specific location allows for more flexibility in the molecule's structure due to the C^5-C^6 bond rotation, resulting in greater affinity for the RP stationary phase and thus slower elution. This assumption is further supported by the chromatographic behaviour of caffeoyl glucosides reported by Jaiswal et al. [49] and Patras et al.[50] . In their study, the 6-caffeoyl glucose isomer consistently eluted later than the other isomers, regardless of the considered anomer. The tandem MS spectra of all five precursor ions $[GA_1\text{-GP-H}]^-$ at *m/z* 331.067 are displayed in **Figure S8**. The predominant product ion at *m/z* 169.015, corresponding to deprotonated gallic acid (GA), was found in all five MS/MS spectra. The product ion at *m/z* 271.047 was absent only in chromatographic peak #5, likely due to the gas-phase neutral loss of $C_2H_4O_2$ (60.021 Da), which involves the C^5 and C^6 positions on the core (**Figure S9**). This fragmentation process cannot occur for the *E* isomer shown in **Figure S7**. The MS/MS spectrum aligns with the difference in retention time noted for the last eluting isomer among those with *m/z* 331.067. It is important to note that the MS/MS data for caffeoyl glucoside isomers reported by Jaiswal et al. [49] and Patras et al.[50] do not fully align with our findings. In their studies, a significant loss of $C_2H_4O_2$ (60 Da) was observed for both anomers of 6-caffeoylglucose, which conflicts with our proposed interpretation. We must consider the structural differences between caffeoyl and gallic acid, as well as variations in the fragmentation energy since the authors employed a CID cell of an ion-trap mass spectrometer. Therefore, injections of standard compounds are necessary to confirm these hypotheses and ensure accurate identification.

Finally, the intensity variation of the *m/z* 211.025 product ions across spectra A to D, and its absence in spectrum E, provides intriguing insights. The neutral loss of 120.042 Da ($C_4H_8O_4$) from the precursor ion leading to that ion is common in glucopyranose fragmentation [51] and could also result in the loss of consecutive $C_2H_4O_2$ units (i.e., 60.0211 Da) [52]. As the number of GA molecules bound to the GP core increases, the complexity of the studied system significantly rises. In **Figure 6A,** the EICC obtained in negative polarity at *m/z* 483.078 (blue), corresponding to [GA_2-GP–H]$^-$] ions, reveals at least fourteen chromatographic peaks (#1h, #2h, ... #14h). Since the theoretically expected number of ten regioisomers is exceeded, these results suggest that GA may be bound to the GP core via one of its phenolic OH groups, or that multiple GA molecules are linked together with ester and ether bonds. Furthermore, several anomeric forms might also be present. The heatmap in **Figure 7** provides an overview of the tandem MS spectra obtained for each chromatographic peak of GA_2-GP and GA_3-GP species. In most cases, the product ion at *m/z* 169.015 [GA-H]$^-$ was the most abundant. However, an intriguing mismatch was observed for the chromatographic peak labelled #7h, where the base peak was found at *m/z* 331.067. The formation of this ion may be due to the neutral loss of a GAk, suggesting a chemical bond between two gallic acid (GA) moieties. Regarding peaks #8b and #9b, an interesting inference can be made concerning the vacant positions at C^6 due to the previously described loss of 60.0 Da, which generated the base peak at *m/z* 423.058. Furthermore, the ion at *m/z* 439.089 was observed as the base peak for #12h and #13h, likely arising from the loss of CO_2 [53], indicating the binding of gallic acid (GA) via one of the phenolic oxygens, as reported in previous studies [54]. Indeed, in the 483.0 > 439.0 MS^3 spectrum obtained for species #13h (**Figure S10**), the intense signal at *m/z* 313.3 possibly results from the loss of the remaining portion of GA, while *m/z* 287.0 may be due to the loss of the other

intact GA. This possibility further adds complexity to the characterization of ETs.

The search for trigalloyl glucopyranosides ($[GA_3\text{-GP-H}]^-$, *m/z* 635.089) revealed five distinct chromatographic peaks, highlighted in orange in **Figure 6B** (peaks #1i-#5i). Through the analysis of standard compounds, peak #4i was readily identified as 1,3,6-trigalloyl glucopyranoside (^{1,3,6}GA-GP). However, the tandem MS spectra, presented as a heatmap in **Figure 7**, could not provide definitive information about the regiochemistry of the other trigalloyl glucopyranosides.

As the number of GA groups increases, the available MS and tandem MS data becomes more limited. For instance, the EICC at *m/z* 787.100 $[GA_4\text{-GP-H}]^-$ shown in **Figure 6B** (blue trace), exhibited two relatively broad chromatographic peaks. The corresponding MS/MS spectra, reported in **Figure S11**, were very similar, with a weak but consistent peak signal found at *m/z* 483.078, resulting from the gas-phase formation of a digalloyl glucopyranoside analogue, which was the precursor, through water loss, of the ion at *m/z* 465.068, having a much higher abundance in both cases.

Pentagalloyl-GP (GA_5-GP) is an important compound with a broad range of anticancer activities [55]. As expected, in the ethanol extract of dried walnut shells a single broadened and relatively intense peak was observed at *m/z* 939.111 as $[M\text{-H}]^-$. Besides the deprotonated molecule, a doubly charged signal at *m/z* 469.052 ($[M\text{-2H}]^{2-}$) was detected.

3.3. Quantitative analyses of ETs in extracts of dried walnut shells

Table 2 presents a detailed summary of the ET content in powdered extracts of dried walnut shells. For quantification, peak area integration covered all isomers shown in **Figures 2** and **6**, excluding peaks not identified as ETs. To quantify the ETs in these extracts, we used GA_3-GP as the standard and employed external calibration (see **Figure S12**). This approach assumes

consistent ionization yield across all ETs and negligible matrix effects. Although this assumption carries some risk, especially since HHDP groups in certain structures can significantly impact ionization efficiency, the primary goal is to highlight the potential of using walnut shell waste as a valuable resource, rather than providing absolute quantitative data.

Under the experimental conditions used in the present work, the limit of detection (LOD) and the limit of quantification (LOQ) of GA_3-GP were 0.64 µM and 2.13 µM, respectively. The ET content in our extracts (between 2.5 and 18.0 µM) fell within the linear range. The analysis revealed that the dried walnut shell extract contained an impressive amount of ETs, translating to over 400 mg of these valuable compounds per 10 g of sample. This finding is particularly noteworthy as it highlights the significant potential of this often-neglected waste byproduct as a rich source of ETs. We wish to emphasize that these data serve as informative indicators, providing valuable insights into the ETs content present within the examined walnut shell byproduct. However, it is crucial to recognize that variations in cultivars or extraction methodologies could introduce nuanced differences in the present results, adding layers of complexity and intrigue to the analysis.

This study explored the hidden riches of ETs within dried walnut shell extracts by RPLC-ESI-MS and tandem MS. ETs presented a big challenge due to several isomeric species. However, considering all the ETs types together, we roughly estimate that 10 g of walnut shell extract contains around 400 mg of these beneficial compounds. This study lays the groundwork for future research aimed at enhancing experimental conditions and providing valuable insights into ETs characterization and separation trying to quantify each specific compound with appropriate standards not yet available. Improved methodologies have the potential to guide strategies for recovering high-value compounds from walnut shells,

transforming them from waste products into valuable resources for a more sustainable green economy in the future.

ACKNOWLEDGMENTS

This work was supported by the project PON Ricerca E Innovazione– Azione IV.6 “Contratti di ricerca su tematiche Green” - 2014-2020 DM 10/08/2021 N.1062 MISURA GREEN H95F21001190006, 02-G-14853-2, financed by the MIUR, and PONa3_00395/1 “BIOSCIENZE & SALUTE (B&H)” of Italian Ministero per l'Istruzione, l'Università e la Ricerca (MIUR). Davide Blasi was acknowledged for the preparation of samples, while Giuseppe Carbone was acknowledged for his support in running some experiments.

SUPPORTING INFORMATION STATEMENT

The supporting information includes schematized structures of isomers of $HHDP_2$-GP (Figure S1) and GA_1-GP (Figure S7). Figure S2 features the Multi-EIC chromatogram obtained in positive ion mode of the ions observed in the ESI-(+) Full MS spectrum of $HHDP_2$-GP. Figure S3 and Figure S11 report tandem MS spectra for two $HHDP_2$-GP and GA_4-GP isobaric species, respectively. Figure S4 and Figure S5 present tandem MS spectra for different isomers of HHDP-GP, and HHDP-GA_3-GP, respectively. Figure S6 shows EIC chromatograms for deprotonated ellagic acid, both as a standard and in the sample. Figure S8 details the MS/MS spectra of five GA_1-GP isomers, with hypothesized structures of fragments shown in Figure S9. Figure S10 provides an MS^3 spectrum suggesting that two GA residues are bound together in a GA_2-GP isomer. Figure S12 shows the linear calibration curve of GA3-GP in the range 1.0–20.0 µM.

REFERENCES

(1) Sagar, N. A.; Pareek, S.; Sharma, S.; Yahia, E. M.; Lobo, M. G. Fruit and Vegetable Waste: Bioactive Compounds, Their Extraction, and Possible Utilization. *Compr. Rev. Food Sci. Food Saf.* **2018**, *17* (3), 512–531. https://doi.org/10.1111/1541-4337.12330.

(2) Carmona-Cabello, M.; Garcia, I. L.; Leiva-Candia, D.; Dorado, M. P. Valorization of Food Waste Based on Its Composition through the Concept of Biorefinery. *Curr. Opin. Green Sustain. Chem.* **2018**, *14*, 67–79. https://doi.org/10.1016/j.cogsc.2018.06.011.

(3) Ogunmakinde, O. E.; Sher, W.; Egbelakin, T. Circular Economy Pillars: A Semi-Systematic Review. *Clean Technol. Environ. Policy* **2021**, *23* (3), 899–914. https://doi.org/10.1007/s10098-020-02012-9.

(4) Casiello, M.; Savino, S.; Massaro, M.; Liotta, L. F.; Nicotra, G.; Pastore, C.; Fusco, C.; Monopoli, A.; D'Accolti, L.; Nacci, A.; Riela, S. Multifunctional Halloysite and Hectorite Catalysts for Effective Transformation of Biomass to Biodiesel. *Appl. Clay Sci.* **2023**, *242*. https://doi.org/10.1016/j.clay.2023.107048.

(5) Craig, W. J. Phytochemicals: Guardians of Our Health. *J. Am. Diet. Assoc.* **1997**, *97* (10 Suppl 2). https://doi.org/10.1016/s0002-8223(97)00765-7.

(6) Renard, C. M. G. C. Extraction of Bioactives from Fruit and Vegetables: State of the Art and Perspectives. *Lwt* **2018**, *93* (March), 390–395. https://doi.org/10.1016/j.lwt.2018.03.063.

(7) Casas-Agustench, P.; Salas-Huetos, A.; Salas-Salvadó, J. Mediterranean Nuts: Origins, Ancient Medicinal Benefits and Symbolism. *Public Health Nutr.* **2011**, *14* (12 A), 2296–2301. https://doi.org/10.1017/S1368980011002540.

(8) Queirós, C. S. G. P.; Cardoso, S.; Lourenço, A.; Ferreira, J.; Miranda, I.; Lourenço, M. J. V; Pereira, H. Characterization of Walnut, Almond, and Pine Nut Shells Regarding Chemical Composition and Extract Composition. *Biomass Convers. Biorefinery* **2020**, *10* (1), 175–188. https://doi.org/10.1007/s13399-019-00424-2.

(9) Salas-Salvadó, J.; Casas-Agustench, P.; Salas-Huetos, A. Cultural and Historical Aspects of Mediterranean Nuts with Emphasis on Their Attributed Healthy and Nutritional Properties. *Nutr. Metab. Cardiovasc. Dis.* **2011**, *21* (SUPPL. 1). https://doi.org/10.1016/j.numecd.2010.10.013.

(10) Cerdá, B.; Tomás-Barberán, F. A.; Espín, J. C. Metabolism of Antioxidant and Chemopreventive Ellagitannins from Strawberries, Raspberries, Walnuts, and Oak-Aged Wine in Humans: Identification of Biomarkers and Individual Variability. *J. Agric. Food Chem.* **2005**, *53* (2), 227–235. https://doi.org/10.1021/jf049144d.

(11) Regueiro, J.; Sánchez-González, C.; Vallverdú-Queralt, A.; Simal-Gándara, J.; Lamuela-Raventós, R.; Izquierdo-Pulido, M. Comprehensive Identification of Walnut Polyphenols by

Liquid Chromatography Coupled to Linear Ion Trap-Orbitrap Mass Spectrometry. *Food Chem.* **2014**, *152*, 340–348. https://doi.org/10.1016/j.foodchem.2013.11.158.

(12) Slatnar, A.; Mikulic-Petkovsek, M.; Stampar, F.; Veberic, R.; Solar, A. Identification and Quantification of Phenolic Compounds in Kernels, Oil and Bagasse Pellets of Common Walnut (Juglans Regia L.). *Food Res. Int.* **2015**, *67*, 255–263. https://doi.org/10.1016/j.foodres.2014.11.016.

(13) Quideau, S. Chemistry and Biology of Ellagitannins: An Underestimated Class of Bioactive Plant Polyphenols. *Chem. Biol. Ellagitannins An Underestimated Cl. Bioact. Plant Polyphenols* **2009**, 1–374. https://doi.org/10.1142/6795.

(14) Haslam, E.; Cai, Y. Plant Polyphenols (Vegetable Tannins): Gallic Acid Metabolism. *Nat. Prod. Rep.* **1994**, *11*, 41–66. https://doi.org/10.1039/NP9941100041.

(15) Quideau, S.; Feldman, K. S. Ellagitannin Chemistry. *Chem. Rev.* **1996**, *96* (1), 475–503. https://doi.org/10.1021/cr940716a.

(16) Khanbabaee, K.; van Ree, T. Tannins: Classification and Definition. *Nat. Prod. Rep.* **2001**, *18* (6), 641–649. https://doi.org/10.1039/b101061l.

(17) Sánchez-González, C.; Ciudad, C. J.; Noé, V.; Izquierdo-Pulido, M. Health Benefits of Walnut Polyphenols: An Exploration beyond Their Lipid Profile. *Crit. Rev. Food Sci. Nutr.* **2017**, *57* (16), 3373–3383. https://doi.org/10.1080/10408398.2015.1126218.

(18) Landete, J. M. Ellagitannins, Ellagic Acid and Their Derived Metabolites: A Review about Source, Metabolism, Functions and Health. *Food Res. Int.* **2011**, *44* (5), 1150–1160. https://doi.org/10.1016/j.foodres.2011.04.027.

(19) Garcia-Muñoz, C.; Vaillant, F. Metabolic Fate of Ellagitannins: Implications for Health, and Research Perspectives for Innovative Functional Foods. *Crit. Rev. Food Sci. Nutr.* **2014**, *54* (12), 1584–1598. https://doi.org/10.1080/10408398.2011.644643.

(20) Larrosa, M.; Tomás-Barberán, F. A.; Espín, J. C. The Dietary Hydrolysable Tannin Punicalagin Releases Ellagic Acid That Induces Apoptosis in Human Colon Adenocarcinoma Caco-2 Cells by Using the Mitochondrial Pathway. *J. Nutr. Biochem.* **2006**, *17* (9), 611–625. https://doi.org/10.1016/j.jnutbio.2005.09.004.

(21) Larrosa, M.; González-Sarrías, A.; García-Conesa, M. T.; Tomás-Barberán, F. A.; Espín, J. C. Urolithins, Ellagic Acid-Derived Metabolites Produced by Human Colonic Microflora, Exhibit Estrogenic and Antiestrogenic Activities. *J. Agric. Food Chem.* **2006**, *54* (5), 1611–1620. https://doi.org/10.1021/jf0527403.

(22) Okuda, T.; Yoshida, T.; Hatano, T. Hydrolyzable Tannins and Related Polyphenols. *Fortschritte der Chemie Org. Naturstoffe. Prog. Chem. Org. Nat. Prod. Progrès dans la Chim. des Subst. Org. Nat.* **1995**, *66*, 1–117. https://doi.org/10.1007/978-3-7091-9363-1_1.

(23) Okuda, T. Systematics and Health Effects of Chemically Distinct Tannins in Medicinal Plants. *Phytochemistry* **2005**, *66* (17 SPEC. ISS.), 2012–2031. https://doi.org/10.1016/j.phytochem.2005.04.023.

(24) Tisserant, A.; Pauliuk, S.; Merciai, S.; Schmidt, J.; Fry, J.; Wood, R.; Tukker, A. Solid Waste and the Circular Economy: A Global Analysis of Waste Treatment and Waste Footprints. *J. Ind. Ecol.* **2017**, *21* (3), 628–640. https://doi.org/10.1111/jiec.12562.

(25) Schmidt, O. T. Gallotannine Und Ellagen-Gerbstoffe. *Fortschritte der Chemie Org. Naturstoffe / Prog. Chem. Org. Nat. Prod. / Progrès dans la Chim. des Subst. Org. Nat.* **1956**, 70–136. https://doi.org/10.1007/978-3-7091-8032-7_2.

(26) Yoshida, T.; Amakura, Y.; Yoshimura, M. Structural Features and Biological Properties of Ellagitannins in Some Plant Families of the Order Myrtales. *Int. J. Mol. Sci.* **2010**, *11* (1), 79–106. https://doi.org/10.3390/ijms11010079.

(27) García-Villalba, R.; Espín, J. C.; Aaby, K.; Alasalvar, C.; Heinonen, M.; Jacobs, G.; Voorspoels, S.; Koivumäki, T.; Kroon, P. A.; Pelvan, E.; Saha, S.; Tomás-Barberán, F. A. Validated Method for the Characterization and Quantification of Extractable and Nonextractable Ellagitannins after Acid Hydrolysis in Pomegranate Fruits, Juices, and Extracts. *J. Agric. Food Chem.* **2015**, *63* (29), 6555–6566. https://doi.org/10.1021/acs.jafc.5b02062.

(28) Suvanto, J.; Tähtinen, P.; Valkamaa, S.; Engström, M. T.; Karonen, M.; Salminen, J.-P. Variability in Foliar Ellagitannins of Hippophaë Rhamnoides L. and Identification of a New Ellagitannin, Hippophaenin C. *J. Agric. Food Chem.* **2018**, *66* (3), 613–620. https://doi.org/10.1021/acs.jafc.7b04834.

(29) Baert, N.; Karonen, M.; Salminen, J. P. Isolation, Characterisation and Quantification of the Main Oligomeric Macrocyclic Ellagitannins in Epilobium Angustifolium by Ultra-High Performance Chromatography with Diode Array Detection and Electrospray Tandem Mass Spectrometry. *J. Chromatogr. A* **2015**, *1419*, 26–36. https://doi.org/10.1016/j.chroma.2015.09.050.

(30) Gu, D.; Yang, Y.; Bakri, M.; Chen, Q.; Xin, X.; Aisa, H. A. A LC/QTOF–MS/MS Application to Investigate Chemical Compositions in a Fraction with Protein Tyrosine Phosphatase 1B Inhibitory Activity from Rosa Rugosa Flowers. *Phytochem. Anal.* **2013**, *24* (6), 661–670. https://doi.org/10.1002/pca.2451.

(31) Salminen, J.-P.; Ossipov, V.; Haukioja, E.; Pihlaja, K. Seasonal Variation in the Content of Hydrolysable Tannins in Leaves of Betula Pubescens. *Phytochemistry* **2001**, *57* (1), 15–22. https://doi.org/10.1016/S0031-9422(00)00502-1.

(32) Ventura, G.; Mesto, D.; Blasi, D.; Cataldi, T. R. I.; Calvano, C. D. The Effect of Milling on the Ethanolic Extract Composition of Dried Walnut (Juglans Regia L.) Shells. *Int. J. Mol. Sci.* **2023**,

24 (17). https://doi.org/10.3390/ijms241713059.

(33) Blasi, D.; Mesto, D.; Cotugno, P.; Calvano, C. D.; Lo Presti, M.; Farinola, G. M. Revealing the Effects of the Ball Milling Pretreatment on the Ethanosolv Fractionation of Lignin from Walnut and Pistachio Shells. *Green Chem. Lett. Rev.* **2022**, *15* (4), 893–902. https://doi.org/10.1080/17518253.2022.2143244.

(34) Luque de Castro, M. D.; García Ayuso, L. E. ENVIRONMENTAL APPLICATIONS | Soxhlet Extraction. In *Encyclopedia of Separation Science*; Elsevier, 2000; pp 2701–2709. https://doi.org/10.1016/B0-12-226770-2/06681-3.

(35) Schymanski, E. L.; Jeon, J.; Gulde, R.; Fenner, K.; Ruff, M.; Singer, H. P.; Hollender, J. Identifying Small Molecules via High Resolution Mass Spectrometry: Communicating Confidence. *Environ. Sci. Technol.* **2014**, *48* (4), 2097–2098. https://doi.org/10.1021/es5002105.

(36) Guo, X.; Gu, F.; Yang, T.; Shao, Z.; Zhang, Q.; Zhu, J.; Wang, F. Quantitative Conversion of Free, Acid-Hydrolyzable, and Bound Ellagic Acid in Walnut Kernels during Baking. *Food Chem.* **2023**, *400*, 134070. https://doi.org/10.1016/j.foodchem.2022.134070.

(37) Chang, J. H.; Cho, J. H.; Kim, H. H.; Lee, K. P.; Lee, M. W.; Han, S. S.; Lee, D. I. Antitumor Activity of Pedunculagin, One of the Ellagitannin. *Arch. Pharm. Res.* **1995**, *18* (6), 396–401. https://doi.org/10.1007/BF02976342.

(38) Silva, R. M.; Pereira, L. D.; Véras, J. H.; Vale, C. R. do; Chen-Chen, L.; Santos, S. da C. Protective Effect and Induction of DNA Repair by Myrciaria Cauliflora Seed Extract and Pedunculagin on Cyclophosphamide-Induced Genotoxicity. *Mutat. Res. - Genet. Toxicol. Environ. Mutagen.* **2016**, *810*, 40–47. https://doi.org/10.1016/j.mrgentox.2016.10.001.

(39) Fernandes, T. A.; Antunes, A. M. M.; Caldeira, I.; Anjos, O.; de Freitas, V.; Fargeton, L.; Boissier, B.; Catarino, S.; Canas, S. Identification of Gallotannins and Ellagitannins in Aged Wine Spirits: A New Perspective Using Alternative Ageing Technology and High-Resolution Mass Spectrometry. *Food Chem.* **2022**, *382*. https://doi.org/10.1016/j.foodchem.2022.132322.

(40) Campone, L.; Celano, R.; Lisa Piccinelli, A.; Pagano, I.; Carabetta, S.; Sanzo, R. Di; Russo, M.; Ibañez, E.; Cifuentes, A.; Rastrelli, L. Response Surface Methodology to Optimize Supercritical Carbon Dioxide/Co-Solvent Extraction of Brown Onion Skin by-Product as Source of Nutraceutical Compounds. *Food Chem.* **2018**, *269*, 495–502. https://doi.org/10.1016/j.foodchem.2018.07.042.

(41) Lopes, J. F.; Gaspar, E. M. S. M. Simultaneous Chromatographic Separation of Enantiomers, Anomers and Structural Isomers of Some Biologically Relevant Monosaccharides. *J. Chromatogr. A* **2008**, *1188* (1), 34–42. https://doi.org/10.1016/j.chroma.2007.12.016.

(42) Grace, M. H.; Warlick, C. W.; Neff, S. A.; Lila, M. A. Efficient Preparative Isolation and Identification of Walnut Bioactive Components Using High-Speed Counter-Current

Chromatography and LC-ESI-IT-TOF-MS. *Food Chem.* **2014**, *158*, 229–238. https://doi.org/10.1016/j.foodchem.2014.02.117.

(43) Pinheiro, A. J. M. C. R.; Mendes, A. R. S.; Neves, M. D. F. de J.; Prado, C. M.; Bittencourt-Mernak, M. I.; Santana, F. P. R.; Lago, J. H. G.; de Sá, J. C.; da Rocha, C. Q.; de Sousa, E. M.; Fontes, V. C.; Grisoto, M. A. G.; Falcai, A.; Lima-Neto, L. G. Galloyl-Hexahydroxydiphenoyl (HHDP)-Glucose Isolated from Punica Granatum L. Leaves Protects against Lipopolysaccharide (LPS)-Induced Acute Lung Injury in BALB/c Mice. *Front. Immunol.* **2019**, *10* (AUG). https://doi.org/10.3389/fimmu.2019.01978.

(44) Bowers, J. J.; Gunawardena, H. P.; Cornu, A.; Narvekar, A. S.; Richieu, A.; Deffieux, D.; Quideau, S.; Tharayil, N. Rapid Screening of Ellagitannins in Natural Sources via Targeted Reporter Ion Triggered Tandem Mass Spectrometry. *Sci. Rep.* **2018**, *8* (1), 1–10. https://doi.org/10.1038/s41598-018-27708-3.

(45) Shimoda, H.; Tanaka, J.; Kikuchi, M.; Fukuda, T.; Ito, H.; Hatano, T.; Yoshida, T. Walnut Polyphenols Prevent Liver Damage Induced by Carbon Tetrachloride and D-Galactosamine: Hepatoprotective Hydrolyzable Tannins in the Kernel Pellicles of Walnut. *J. Agric. Food Chem.* **2008**, *56* (12), 4444–4449. https://doi.org/10.1021/jf8002174.

(46) Kurokawa, M.; Hozumi, T.; Tsurita, M.; Kadota, S.; Namba, T.; Shiraki, K. Biological Characterization of Eugeniin as an Anti-Herpes Simplex Virus Type 1 Compound in Vitro and in Vivo. *J. Pharmacol. Exp. Ther.* **2001**, *297* (1), 372–379.

(47) Evtyugin, D. D.; Magina, S.; Evtuguin, D. V. Recent Advances in the Production and Applications of Ellagic Acid and Its Derivatives. A Review. *Molecules* **2020**, *25* (12), 2745. https://doi.org/10.3390/molecules25122745.

(48) Gupta, A.; Singh, A. K.; Kumar, R.; Jamieson, S.; Pandey, A. K.; Bishayee, A. Neuroprotective Potential of Ellagic Acid: A Critical Review. *Adv. Nutr.* **2021**, *12* (4), 1211–1238. https://doi.org/10.1093/advances/nmab007.

(49) Jaiswal, R.; Matei, M. F.; Glembockyte, V.; Patras, M. A.; Kuhnert, N. Hierarchical Key for the LC–MS n Identification of All Ten Regio- and Stereoisomers of Caffeoylglucose. *J. Agric. Food Chem.* **2014**, *62* (38), 9252–9265. https://doi.org/10.1021/jf501210s.

(50) Patras, M. A.; Jaiswal, R.; McDougall, G. J.; Kuhnert, N. Profiling and Quantification of Regioisomeric Caffeoyl Glucoses in Berry Fruits. *J. Agric. Food Chem.* **2018**, *66* (5), 1096–1104. https://doi.org/10.1021/acs.jafc.7b02446.

(51) Calvano, C. D.; Cataldi, T. R. I.; Kögel, J. F.; Monopoli, A.; Palmisano, F.; Sundermeyer, J. Structural Characterization of Neutral Saccharides by Negative Ion MALDI Mass Spectrometry Using a Superbasic Proton Sponge as Deprotonating Matrix. *J. Am. Soc. Mass Spectrom.* **2017**, *28* (8), 1666–1675. https://doi.org/10.1007/s13361-017-1679-y.

(52) Giangrande, C.; Auberger, N.; Rentier, C.; Papini, A. M.; Mallet, J.-M.; Lavielle, S.; Vinh, J. Multi-Stage Mass Spectrometry Analysis of Sugar-Conjugated β-Turn Structures to Be Used as Probes in Autoimmune Diseases. *J. Am. Soc. Mass Spectrom.* **2016**, *27* (4), 735–747. https://doi.org/10.1007/s13361-015-1321-9.

(53) Ventura, G.; Calvano, C. D.; Abbattista, R.; Bianco, M.; De Ceglie, C.; Losito, I.; Palmisano, F.; Cataldi, T. R. I. Characterization of Bioactive and Nutraceutical Compounds Occurring in Olive Oil Processing Wastes. *Rapid Commun. Mass Spectrom.* **2019**, *33* (21), 1670–1681. https://doi.org/10.1002/rcm.8514.

(54) Santos, S. A. O.; Vilela, C.; Freire, C. S. R.; Neto, C. P.; Silvestre, A. J. D. Ultra-High Performance Liquid Chromatography Coupled to Mass Spectrometry Applied to the Identification of Valuable Phenolic Compounds from Eucalyptus Wood. *J. Chromatogr. B Anal. Technol. Biomed. Life Sci.* **2013**, *938*, 65–74. https://doi.org/10.1016/j.jchromb.2013.08.034.

(55) Wen, C.; Dechsupa, N.; Yu, Z.; Zhang, X.; Liang, S.; Lei, X.; Xu, T.; Gao, X.; Hu, Q.; Innuan, P.; Kantapan, J.; Lü, M. Pentagalloyl Glucose: A Review of Anticancer Properties, Molecular Targets, Mechanisms of Action, Pharmacokinetics, and Safety Profile. *Molecules* **2023**, *28* (12), 4856. https://doi.org/10.3390/molecules28124856.

This is a pre-print version associated to paper with doi: **10.1021/acs.jafc.4c05146**

FIGURE CAPTIONS

Figure 1. Structure of an HHDP-trigalloyl glucopyranose.ù

Figure 2. Representative EIC chromatogram by RPLC-ESI(-)-FTMS of a sample extract of dried powdered walnut shells. The current extraction window was set up to 5 ppm, centred on the theoretical m/z ratios of (A) $HHDP_2$-GP at *m/z* 783.069 (orange), HHDP-GP at *m/z* 481.062 (blue), and HHDP-GA-GP at *m/z* 633.073 (green) as deprotonated species ($[M-H]^-$). EICC of (B) $HHDP_2$ GA-GP at *m/z* 935.080 and *m/z* 467.036 as doubly charged (orange), HHDP-GA_2-GP at *m/z* 785.084 (blue), and HHDP-GA_3-GP at *m/z* 937.095 and *m/z* 468.044 as doubly charged (green). Isomers are labelled by the same letter and increasing number. The asterisked peak (*) is due to the isobaric M+2 ion of a more oxidated species.

Figure 3. Tandem MS spectra of precursor ions at *m/z* 783.069 under chromatographic peaks labelled as #3a (A) and #4a (B) in **Figure 2A**, corresponding to deprotonated $HHDP_2$-GP. Putative structures for ions detected at *m/z* 300.999 and *m/z* 275.020 are reported as insets.

Figure 4. Relative abundances and *m/z* values of product ions detected by HCD tandem MS of the precursor ions at *m/z* 633.073 (HHDP-GA-GP) and *m/z* 785.084 ($HHDP_2$-GA-GP). The colour code indicates the significance of each product ion in the spectrum, with intensity decreasing from green to red.

Figure 5. Tandem MS spectra referred to chromatographic peaks labelled as #1d (A) and #2d (B) in Figure 2B, corresponding to deprotonated species of isomeric $HHDP_2$-GA-GP (*m/z* 935.080)

Figure 6. Representative EIC chromatogram by RPLC-ESI(-)-FTMS of a sample extract of dried powdered walnut shells. The current extraction window was set up to 5 ppm, centred on the theoretical m/z ratios of deprotonated ETs (A) GA_1-GP at *m/z* 331.067 (orange) and GA_2-GP at *m/z* 483.078 (blue); (B) GA_3-GP at *m/z* 635.089, GA_4-GP at *m/z* 787.100 (green trace), and GA_5-GP at *m/z* 939.111 (blue trace) also including the EIC at *m/z* 469.052 (i.e. $[GA_5\text{-GP} - 2H]^{2-}$). Isomers are labelled by the same letter and increasing number. The asterisked peaks (*) are due to the isobaric M+2 ion of a more oxidated species.

623 **Figure 7.** Relative abundances and *m/z* values of product ions detected by HCD tandem MS of the precursor ions
624 at *m/z* 483.078 (GA_2-GP), and *m/z* 635.089 (GA_3-GP). The colour code indicates the significance of each product
625 ion in the spectrum, with intensity decreasing from green to red.

TABLES

Table 1. Putative ETs corresponding to GP linked to different numbers of galloyl units found in extracts of dried powdered walnut shells investigated by RPLC-ESI(-)-MS and tandem MS.

GA [a]	Name	Condensed Name	Chemical Formula (M)	*n* [b]	$[M-H]^-$ *m/z*
1	Monogalloyl GPs	GA_1-GPs	$C_{13}H_{16}O_{10}$	5	331.067
2	Digalloyl GPs	GA_2-GPs	$C_{20}H_{20}O_{14}$	10	483.078
3	Trigalloyl GPs	GA_3-GPs	$C_{27}H_{24}O_{18}$	10	635.089
4	Tetragalloyl GPs	GA_4-GPs	$C_{34}H_{28}O_{22}$	5	787.100
5	Pentagalloyl GP	GA_5-GP	$C_{41}H_{32}O_{26}$	1	939.111

[a] Gallic acid (GA) esterified with the glucopyranoside core. [b] Number of isomers. Anomers were not included in the calculation.

Table 2. Quantitative data of ETs in extracts of dried walnut shells, with values reported in micromolar concentration (μM) and milligrams (mg) per g of dried sample. ETs with relatively high content are in bold.

Ellagitannins	Formula (M)	$[M-H]^-$ *m/z*	Concentration (μM)[a]	mg/g of dried walnut shells
GA_1-GP	$C_{13}H_{16}O_{10}$	331.067	2.26 ± 0.10	0.50 ± 0.02
GA_2-GP	$C_{20}H_{20}O_{14}$	483.078	3.59 ± 0.02	1.16 ± 0.01
GA_3-GP	$C_{27}H_{24}O_{18}$	635.089	3.06 ± 0.07	1.29 ± 0.03
GA_4-GP	$C_{34}H_{28}O_{22}$	787.100	2.92 ± 0.08	1.53 ± 0.04
GA_5-GP	$C_{41}H_{32}O_{26}$	**939.111**	**8.32 ± 0.05**	**5.21 ± 0.03**
$HHDP_1$-GP	$C_{20}H_{18}O_{14}$	481.062	14.45 ± 0.03	4.63 ± 0.01
$HHDP_1$-GA_1-GP	$C_{27}H_{22}O_{18}$	633.073	8.30 ± 0.05	3.50 ± 0.02
$HHDP_1$-GA_2-GP	$C_{34}H_{26}O_{22}$	785.084	7.23 ± 0.05	3.78 ± 0.02
$HHDP_2$-GP	$C_{34}H_{24}O_{22}$	**783.069**	**17.28 ± 0.03**	**9.02 ± 0.01**
$HHDP_1$-GA_3-GP	$C_{41}H_{30}O_{26}$	937.095	3.90 ± 0.06	2.43 ± 0.04
$HHDP_2$-GA_1-GP	$C_{41}H_{28}O_{26}$	**935.080**	**11.49 ± 0.03**	**7.16 ± 0.02**

[a] The concentrations refer to injected samples. Three injection replicates were analyzed. Data are reported as mean ± standard deviation.

This is a pre-print version associated to paper with doi: **10.1021/acs.jafc.4c05146**

FIGURES

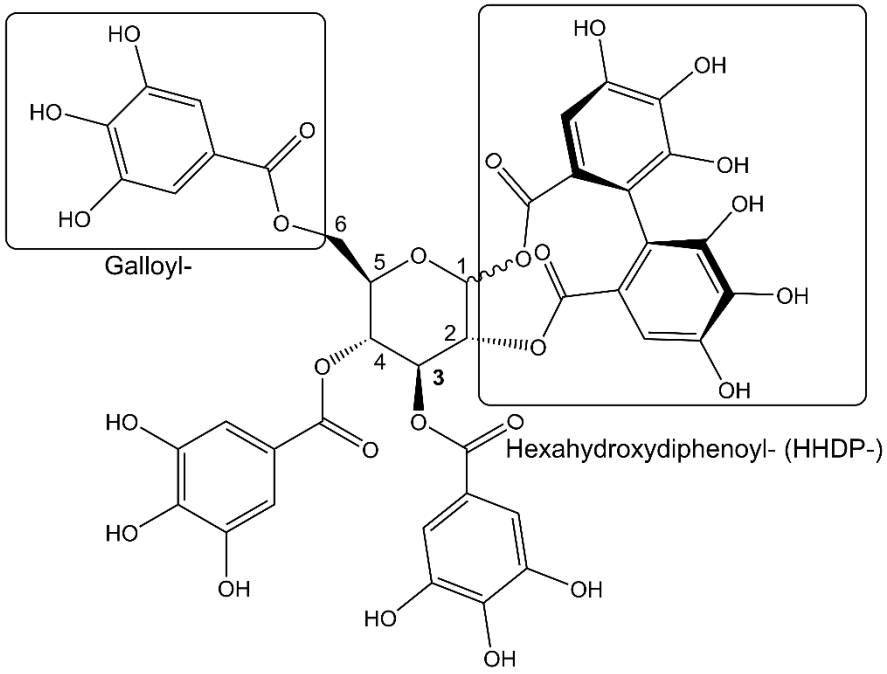

Figure 1

This is a pre-print version associated to paper with doi: **10.1021/acs.jafc.4c05146**

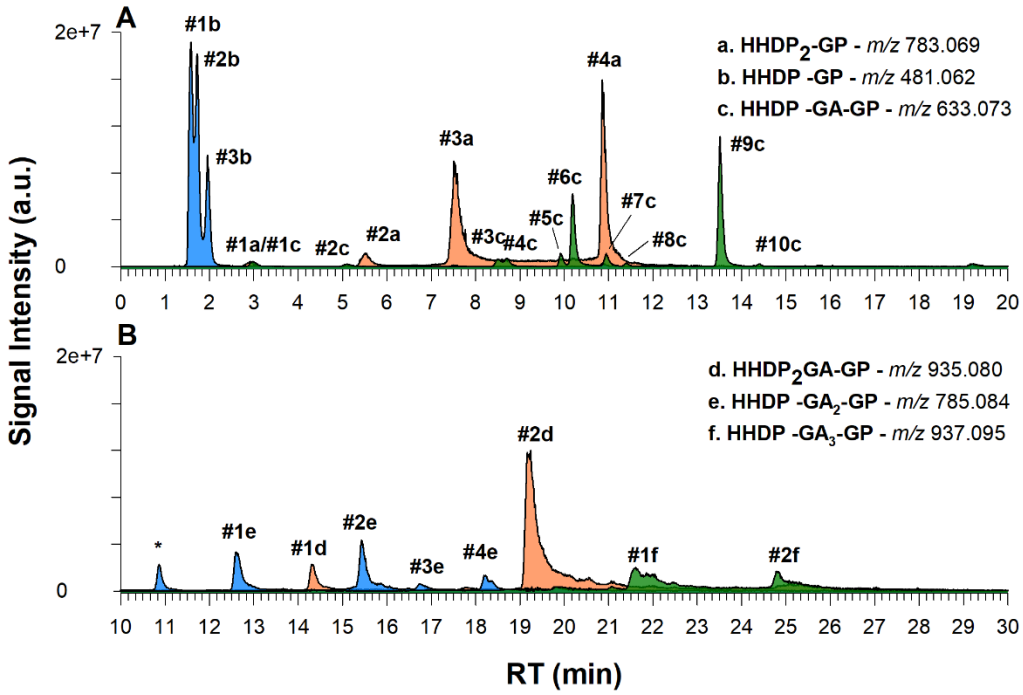

Figure 2

This is a pre-print version associated to paper with doi: **10.1021/acs.jafc.4c05146**

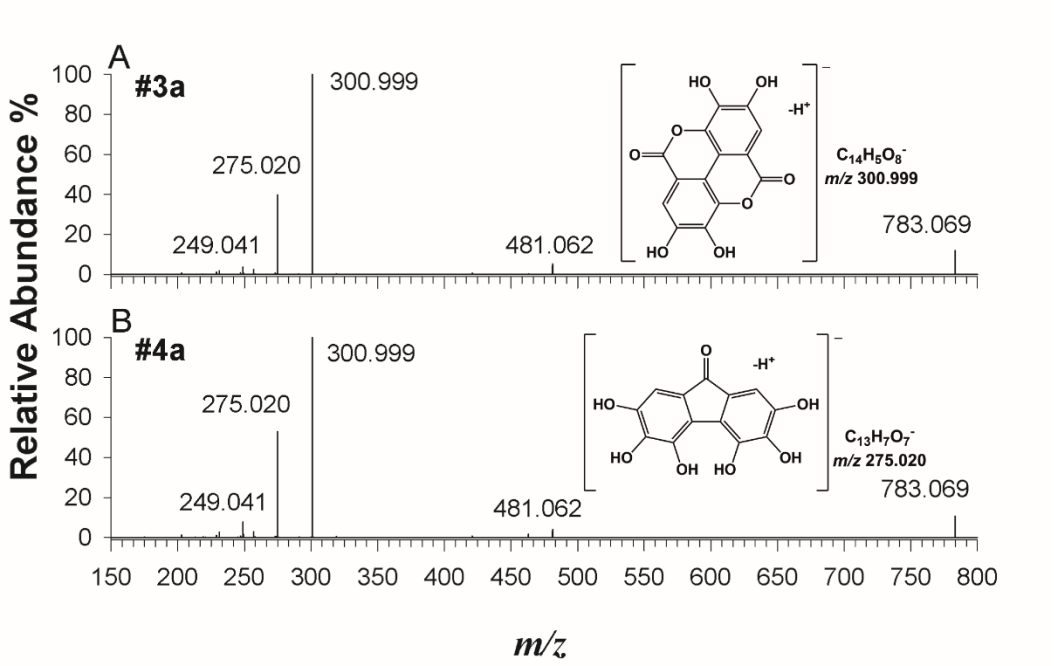

Figure 3

		m/z										
		169.014	249.041	275.020	300.999	421.031	463.053	481.062	483.078	615.063	633.073	785.084
HHDP-GA-GP	#1c	6.0	26.0	49.7	100.0	0.0	0.0	9.2			30.4	
	#2c	4.8	32.7	52.1	100.0	0.0	0.0	6.7			27.5	
	#3c #4c	5.1	3.9	41.6	100.0	0.0	0.0	6.6			12.3	
	#5c	2.9	3.6	33.0	100.0	5.2	1.4	1.4			12.3	
	#6c	8.3	0.0	20.1	100.0	0.0	6.5	7.8			7.0	
	#7c	3.2	2.8	23.2	100.0	6.3	1.9	1.5			13.0	
	#8c	4.1	1.2	52.9	100.0	1.0	0.0	0.0			27.1	
	#9c	1.8	4.1	12.4	100.0	0.0	5.7	0.5			19.3	
	#10c	0.0	0.0	9.0	100.0	0.0	10.6	0.7			13.3	
HHDP-GA_2-GP	#1e	11.2	31.0	40.5	100.0		0.0		2.5	2.7	3.8	10.8
	#2e	11.4	30.7	36.6	100.0		0.0		2.9	0.0	3.9	8.2
	#3e	10.8	24.7	38.5	100.0		0.0		3.6	0.0	6.6	24.1
	#4e	6.5	13.1	29.5	100.0		1.4		0.0	3.7	2.1	7.2
	#5e	3.5	5.7	17.6	100.0		3.3		0.5	0.0	33.2	2.3

Figure 4

This is a pre-print version associated to paper with doi: **10.1021/acs.jafc.4c05146**

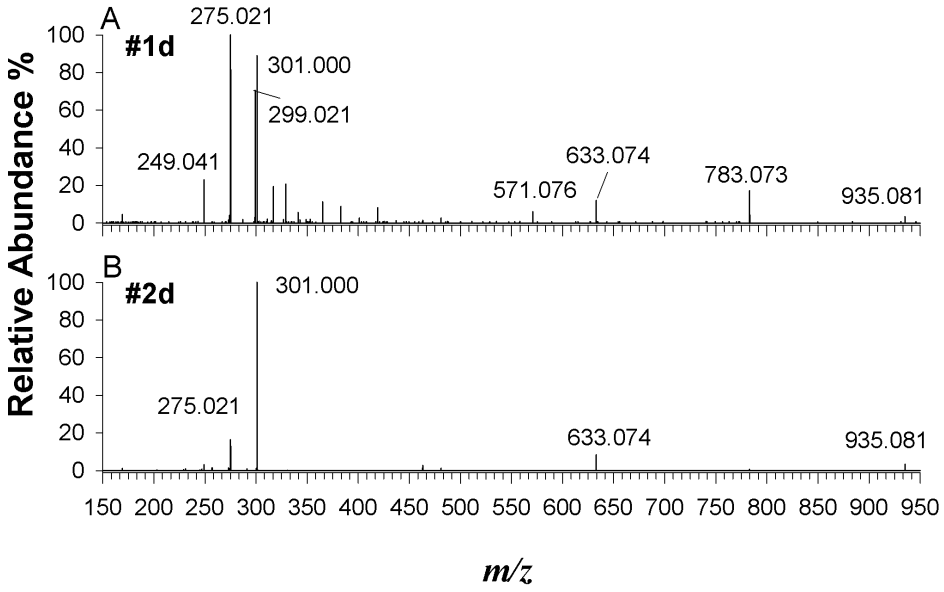

Figure 5

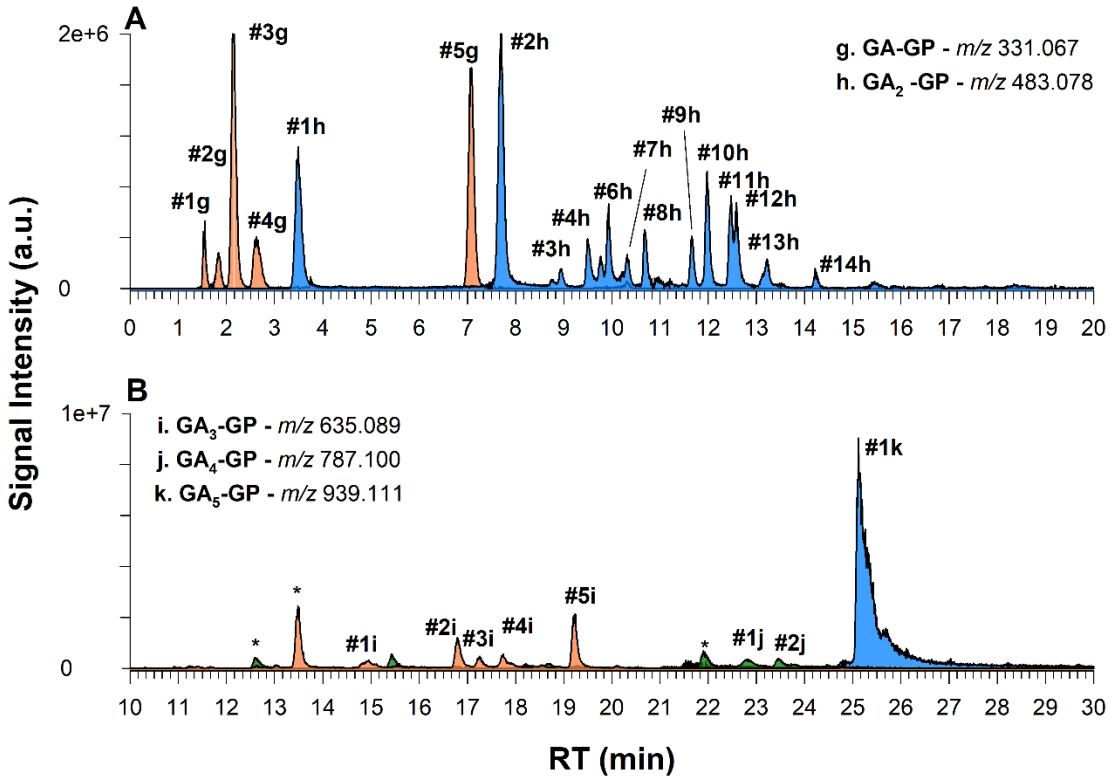
A
2e+6
0
#1g
#2g
#3g
#4g
#1h
#5g
#2h
#3h
#4h
#6h
#7h
#8h
#9h
#10h
#11h
#12h
#13h
#14h
g. GA-GP - m/z 331.067
h. GA2 -GP - m/z 483.078
B
1e+7
0
i. GA3-GP - m/z 635.089
j. GA4-GP - m/z 787.100
k. GA5-GP - m/z 939.111
#1i
#2i
#3i
#4i
#5i
#1j
#2j
#1k
Signal Intensity (a.u.)
RT (min)

Figure 6

		m/z													
		125.025	151.004	169.014	193.015	211.025	241.037	271.046	313.058	331.067	423.058	439.089	465.068	483.078	635.089
GA_2-GP	#1h	17.1	2.9	100.0	0.8	3.5	0.0	0.0	14.3	19.9	0.0	0.0	0.0	27.2	0.0
	#2h	17.4	3.9	100.0	0.9	3.4	0.0	1.3	16.8	25.5	0.0	0.0	0.0	26.3	0.0
	#3h	15.5	0.0	100.0	0.0	0.0	0.0	0.0	0.0	10.2	0.0	0.0	0.0	6.3	0.0
	#4h	13.7	8.5	100.0	0.0	1.3	0.0	0.0	67.8	11.2	0.0	0.0	0	8.3	0
	#5h	16.0	10.5	100.0	0.0	12.1	0.0	7.9	35.5	72.3	0.0	0.0	0	60.9	0
	#6h	13.7	0.0	99.6	31.0	90.0	7.3	100.0	31.7	50.4	0.0	0.0	0.0	26.8	0.0
	#7h	1.1	9.9	32.3	0.0	8.8	0.0	12.0	0.0	100.0	0.0	0.0	0.0	0.0	0.0
	#8h	11.2	0.0	100.0	5.4	37.5	7.3	54.1	9.0	26.9	58.0	0.0	0.0	41.1	0.0
	#9h	9.7	100.0	4.9	45.7	58.7	0.0	0.0	11.9	10.2	62.3	0.0	0.0	49.8	0.0
	#10h	13.7	2.2	100.0	0.0	2.8	0.3	8.1	39.7	3.8	0.0	0.0	0.0	8.6	0.0
	#11h and #12h	10.3	0.0	80.4	17.7	65.4	5.3	100.0	33.4	9.7	0.0	0.0	0.0	47.6	0.0
	#13h	20.1	0.0	100.0	0.0	8.1	3.3	26.9	67.4	19.4	0.0	4.8	0	41.1	0
	#14h	7.8	0.0	100.0	0.0	0.0	0.0	0.0	32.4	0.0	0.0	0.0	0	36.9	0
GA_3-GP	#1i	0.0	0.0	100	0.0	23.64	0.0	19.68	34.66	0.0	22.78	0.0	38.43	29.23	45.89
	#2i	0.0	0.0	57.72	0.0	6.59	0.0	0.0	52.07	0.0	0.0	0.0	100	0.0	0.0
	#3i	0.0	0.0	100	0.0	9.44	0.0	10.09	49.47	0.0	0.0	0.0	68.03	26.37	20.63
	#4i	0.0	0	100	0	25.96	0	34.38	37.83	0	33.65	0	32.29	49.72	63.78
	#5i	0.0	0	100	0	0	0	8.15	50.75	0	8.85	0	59.96	23.56	38.6

Figure 7

This is a pre-print version associated to paper with doi: **10.1021/acs.jafc.4c05146**

TOC GRAPHIC